Interfacial Debonding of Boron Nitride Nanoparticle Reinforced 6061 Aluminum Alloy Matrix Composites

[1] B. Kotiveera Chari and A. Chennakesava Reddy[2]

[1]Professor, Department of Mechanical Engineering, NIT, Warangal, India.
[2]Assistant Professor, Department of Mechanical Engineering, MJ College of Engineering and Technology, Hyderabad, India
dr_acreddy@yahoo.com

Abstract: *A diamond array unit cell/hexagonal BN nanoparticle RVE models were used to predict micromechanical behavior and interfacial debonding in AA6061/BN composites. The AA6061/* BN *particulate metal matrix composites were fabricated at different volume fractions of BN. The uniform distribution of BN nanoparticles in the AA6061 alloy matrix could be attributed to the closer density values between the AA6061 alloy matrix and BN nanoparticles. The interfacial debonding and matrix fracture were observed in the composites.*

Keywords: AA6061*, boron nitride, hexagonal nanoparticle, RVE model, finite element analysis, debonding.*

1. INTRODUCTION

Boron nitride (BN) is an interesting material owing to its unique combination of properties, such as low density, high melting point, high thermal conductivity and high electrical resistivity. Literature studies reveal the positive influence of boron nitride particles on the mechanical properties improvement in aluminum matrix composites [1-3]. The interface reaction is so strenuous that the BN is almost completely consumed, and the interface reaction product is a disadvantage to the mechanical properties of the resulting material. A study was conducted on the silane interfacial effect on the fracture process of embedded single E-glass fiber [4]. The interfacial reinforcement reflects the progressed fracture rather than the instantaneous fracture. A variety of nanoparticles such as silicon nitride [5, 6], titanium oxide [7, 8], graphite [9], titanium carbide [10, 11], boron nitride [12], zirconium oxide [13], titanium nitride [14], titanium boride [15], zirconium carbide [16], silicon oxide [17], magnesium oxide [18] at 10%, 20% and 30% volume fractions were studied and the results computed from a unit cell with uniformly distributed particles were compared. The influence of progressive damage on stress-strain relation of particulate-reinforced composites was studied with two schemes. Finite element analysis for a unit cell containing one particle in a matrix was widely applied to fracture or debonding of particles [19].

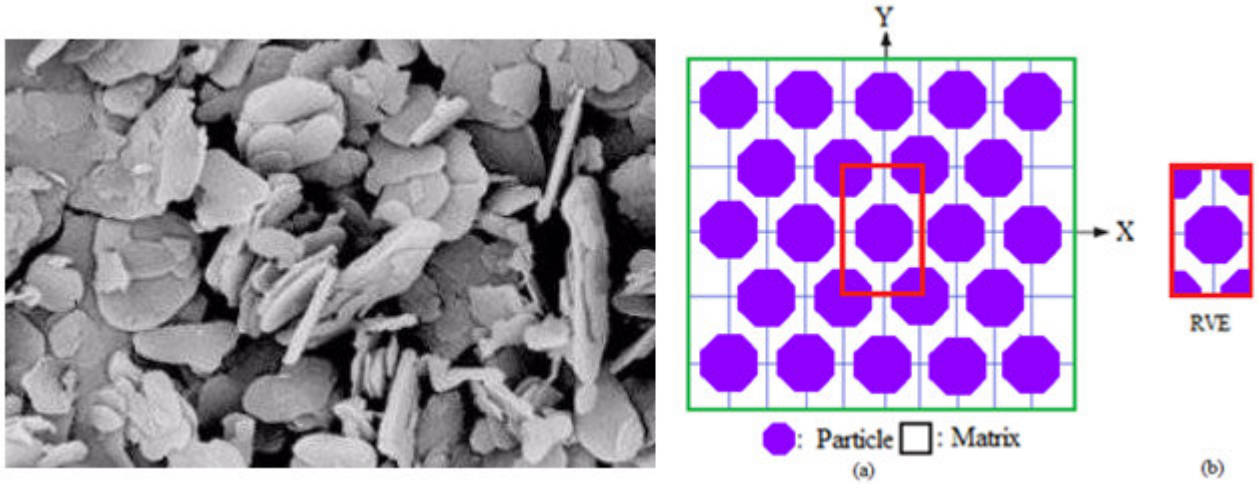

Figure 1: A diamond RVE containing a hexagonal nanoparticle.

In the current work, nano-sized boron nitride particulates were incorporated in AA6061 alloy through the stir casting process. The effect of varying volume fractions of nano-BN addition on the microstructural and mechanical properties of AA6061 alloy is investigated. The structure-property relationship is used to understand the observed mechanical behavior of the developed AA6061 alloy/BN nanocomposites.

Hexagonal boron nitride powder has a structure and properties similar to graphite. It has become one of the most popular dry lubricants due to its lubricating properties and inertness to molten metals and salts. Hexagonal structure boron nitride improves the strength and holdability of the present powder composites. The shape of BN particle considered in this work is an hexagonal. The periodic particle distribution was a diamond array as shown in figure 1.

2. THEORETICAL BACKGROUND

The strains along x- and y-directions can be determined as using the following equations:

$$\varepsilon_y = -\left(\frac{v_{xy}}{E_x} + \frac{1}{E_z}\right) P = \frac{\Delta y}{a} \quad (1)$$

$$\varepsilon_x = \left(\frac{1}{E_x} - \frac{1}{E_z}\right) P = \frac{\Delta x}{a} \quad (2)$$

The effective elastic moduli and Poisson's ratio in the transverse direction (xy-plane) as follows:

$$E_x = \frac{1}{\frac{\Delta x}{Pa} + \frac{1}{E_z}} \text{ and } E_y = \frac{1}{\frac{\Delta y}{Pa} + \frac{1}{E_z}} \quad (3)$$

$$v_{xy} = \left(\frac{\Delta y}{Pa} + \frac{1}{E_z}\right) / \left(\frac{\Delta x}{Pa} + \frac{1}{E_z}\right) \quad (4)$$

Once the change in lengths along x- and y- direction (Δx and Δy) are determined for the square RVE from the FEA, E_y and E_x and v_{xy} can be determined from Eqs. (3) and (4), correspondingly. Considering adhesion, formation of precipitates, particle size, agglomeration, voids/porosity, obstacles to the dislocation, and the interfacial reaction of the particle/matrix, the formula for the strength of composite is stated below:

$$\sigma_c = \left[\sigma_m \left\{\frac{1-(v_p+v_v)^{2/3}}{1-1.5(v_p+v_v)}\right\}\right] e^{m_p(v_p+v_v)} + k d_p^{-1/2} \quad (5)$$

$$k = E_m m_m / E_p m_p$$

where, v_v and v_p are the volume fractions of voids/porosity and nanoparticles in the composite respectively, m_p and m_m are the possion's ratios of the nanoparticles and matrix respectively, d_p is the mean nanoparticle size (diameter) and E_m and E_p is elastic moduli of the matrix and the particle respectively. Elastic modulus (Young's modulus) is a measure of the stiffness of a material and is a quantity used to characterize materials. Elastic modulus is the same in all orientations for isotropic materials. Anisotropy can be seen in many composites.

The upper-bound equation is given by

$$\frac{E_c}{E_m} = \left(\frac{1-v_v^{2/3}}{1-v_v^{2/3}+v_v}\right) + \frac{1+(\delta-1)v_p^{2/3}}{1+(\delta-1)(v_p^{2/3}-v_p)} \quad (6)$$

The lower-bound equation is given by

$$\frac{E_c}{E_m} = 1 + \frac{v_p - v_p}{\delta/(\delta-1)-(v_p+v_v)^{1/3}} \quad (7)$$

where, $\delta = E_p / E_m$.

The transverse modulus is given by

$$E_t = \frac{E_m E_p}{E_m + E_p(1-v_p^{2/3})/v_p^{2/3}} + E_m\left(1 - v_p^{2/3} - v_v^{2/3}\right) \quad (8)$$

3. MATERIALS METHODS

The matrix material was AA6061 alloy. The reinforcement material was hexagonal BN nanoparticles of average size 100nm. The mechanical properties of materials used in the present work are given in table 1.

Table 1: Mechanical properties of AA4015 matrix and BN nanoparticles

Property	AA6061	BN
Density, g/cc	2.70	2.10
Elastic modulus, GPa	68.90	100.00
Ultimate tensile strength, MPa	310	56
Poisson's ratio	0.33	0.27

AA6061 alloy/BN composites were manufactured by the stir casting process and low pressure casting technique with argon gas at 3.0 bar. The composite samples were give solution treatment and cold rolled to the predefined size of tensile specimens. The heat-treated samples were machined to get flat-rectangular specimens (figure 2) for the tensile tests. The tensile specimens

were placed in the grips of a Universal Test Machine (UTM) at a specified grip separation and pulled until failure. The test speed was 2 mm/min (as for ASTM D3039). A strain gauge was used to determine elongation.

In this research, a cubical representative volume element (RVE) was implemented to analyze the tensile behavior AA6061/BN nanoparticle composites at three (10%, 20% and 30%) volume fractions of BN. The large strain PLANE183 element was used in the matrix in all the models. In order to model the adhesion between the matrix and the particle, a CONTACT 172 element was used.

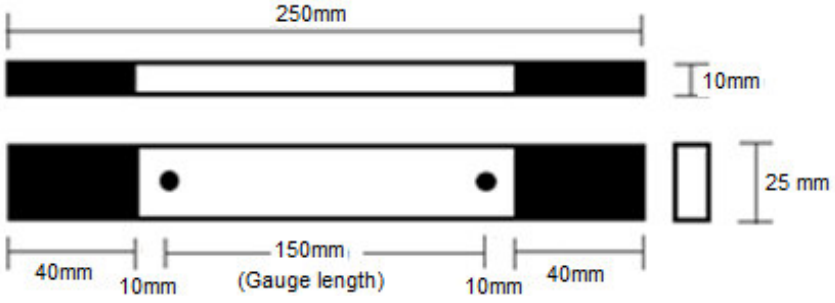

Figure 2: Shape and dimensions of tensile specimen

4. RESULTS AND DISCUSSION

The microstructure as shown in figure 3 indicates a uniform distribution of BN nanoparticles inside the AA6061 alloy matrix. The uniform distribution of BN nanoparticles in the AA6061 alloy matrix could be attributed to the closer density values between the AA6061 alloy matrix (2.7 g/cc) and BN reinforcements (2.1 g/cc), resulting in lesser gravity assisted segregation problems during the blending, stir casting process.

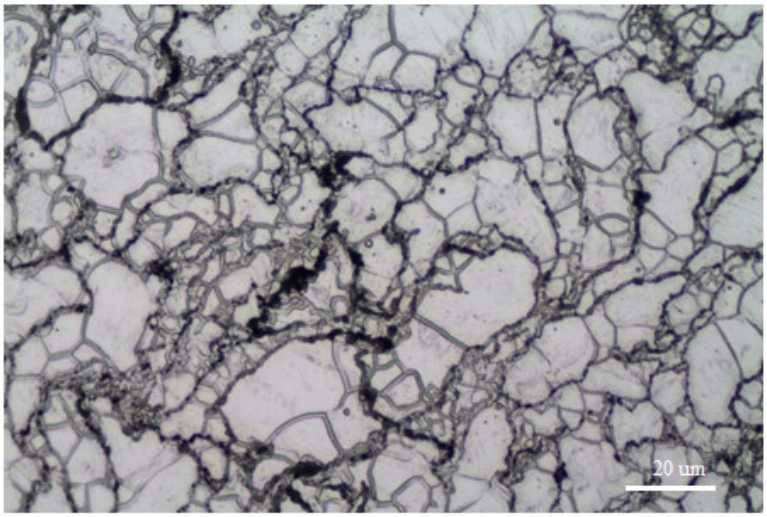

Figure 3: Optical micrographs showing the grain characteristics of AA6061/30% BN composite.

4.1 Micromechanical Behavior

Figure 4a represents the normalized tensile strengths of the AA6061 alloy/BN composites obtained by FEA, present mathematical model, and experimental test. The tensile strength is normalized with ultimate tensile strength of AA6061 alloy. The results are in the acceptable range of computation. The normalized elastic modulus is shown in figure 4b. The elastic modulus is normalized with the elastic modulus of AA6061 alloy. The stiffness of the composites is unchanged with increase of volume fraction of BN. The upper limit (UL) values computed by the present mathematical model are higher than those values obtained by the 'Role of Mixtures (ROM)'and FEA. This is because of assumption of voids and agglomeration in the present mathematical model. The shear strength of the composites is low for the volume fraction of 30% BN (figure 4c). The major Poisson's ratio increases with increase of volume fraction of BN particles (figure 4d).

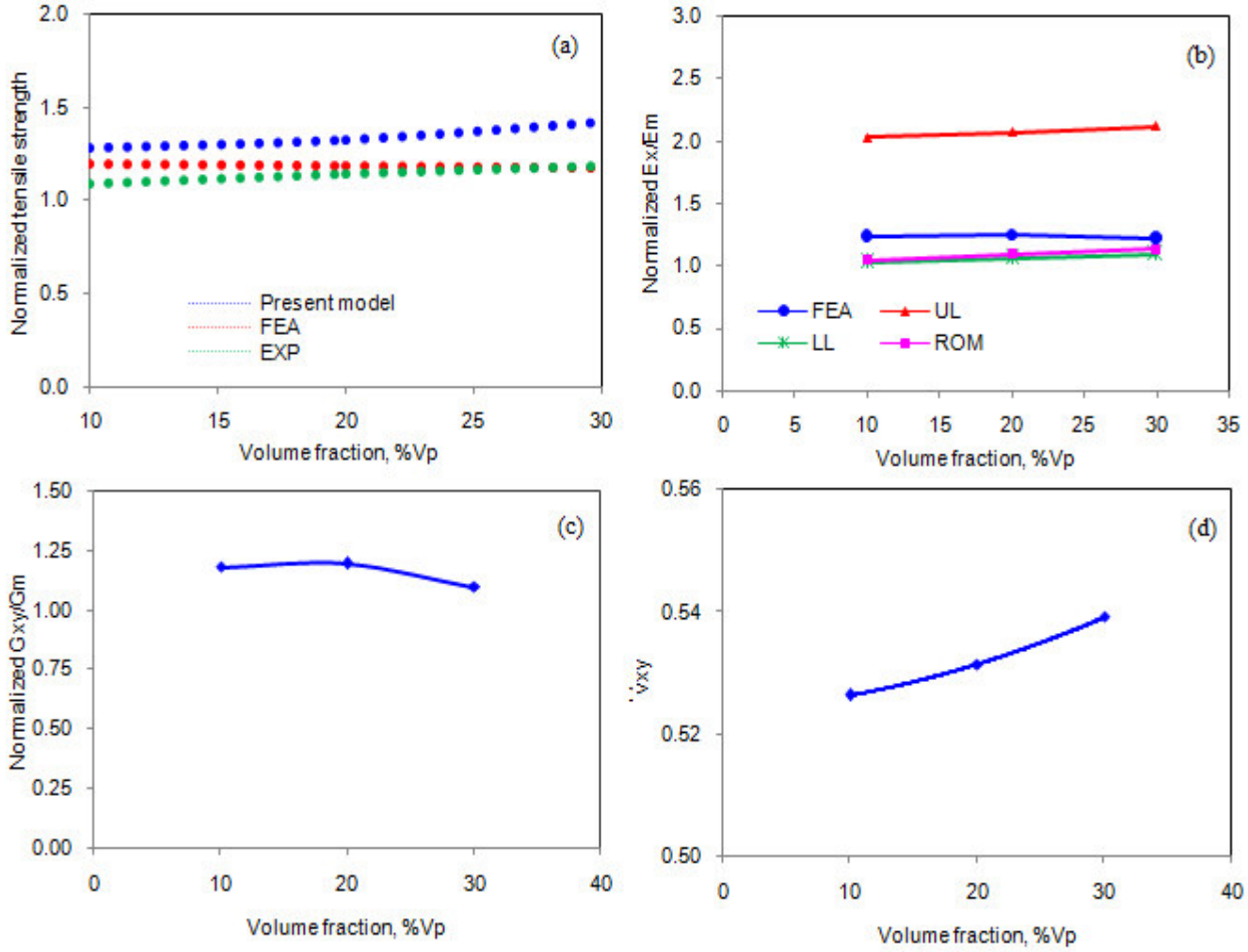

Figure 4: Effect of volume fraction on micromechanical behavior of AA6061/BN composites.

4.2 Fracture Analysis

If the particle deforms in an elastic manner (according to Hooke's law) then,

$$\tau = \frac{n}{2}\sigma_p \quad (9)$$

where σ_p is the particle stress. If particle fracture occurs when the stress in the particle reaches its ultimate tensile strength, $\sigma_{p,uts}$, then setting the boundary condition at

$$\sigma_p = \sigma_{p,\,uts} \quad (10)$$

The relationship between the strength of the particle and the interfacial shear stress is such that if

$$\sigma_{P,uts} < \frac{2\tau}{n} \quad (11)$$

Then the particle will fracture. From the figure 5b, it is observed that the TiC nanoparticle was not fractured as the condition in Eq. (11) is not satisfied. For the interfacial debonding/yielding to occur, the interfacial shear stress reaches its shear strength:

$$\tau = \tau_{max} \quad (12)$$

For particle/matrix interfacial debonding can occur if the following condition is satisfied:

$$\tau_{max} < \frac{n\sigma_p}{2} \quad (13)$$

It is observed from figure 5a that the interfacial debonding occurs between TiC nanoparticle and AA4015 alloy matrix as the condition in Eq.(13) is satisfied.

As seen from figure 6 the shear stress developed at the interface are higher than that induced in the nanoparticle. Hence, the interfacial debonding was occurred between the particle and the matrix. The cleavage mode of fracture is also observed in AA6061 alloy matrix under tensile loading (figure 7).

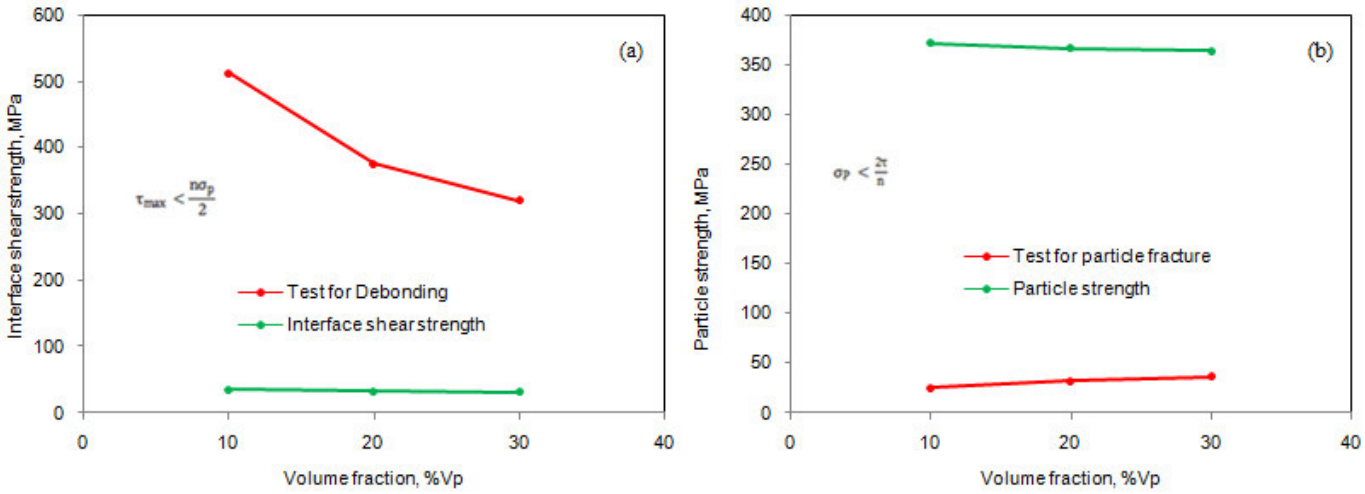

Figure 5: Criterion interfacial debonding (a) and for particle fracture (b).

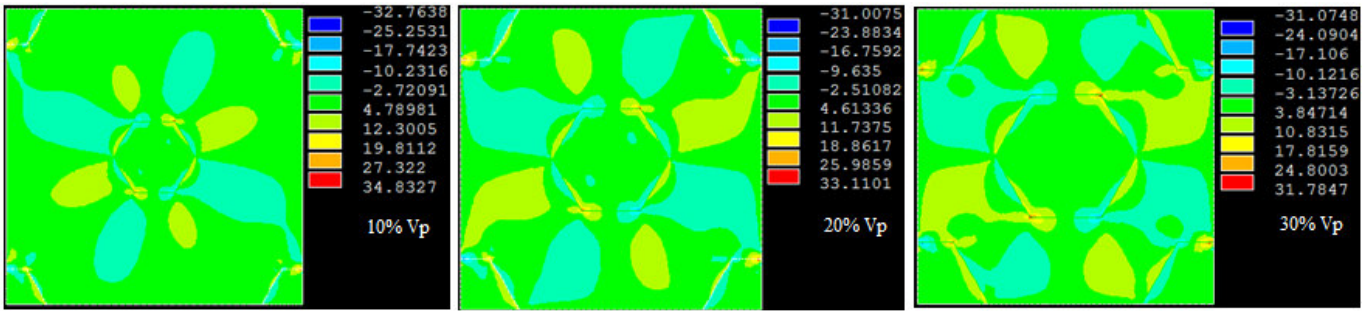

Figure 6: Images of tensile stress obtained from FEA.

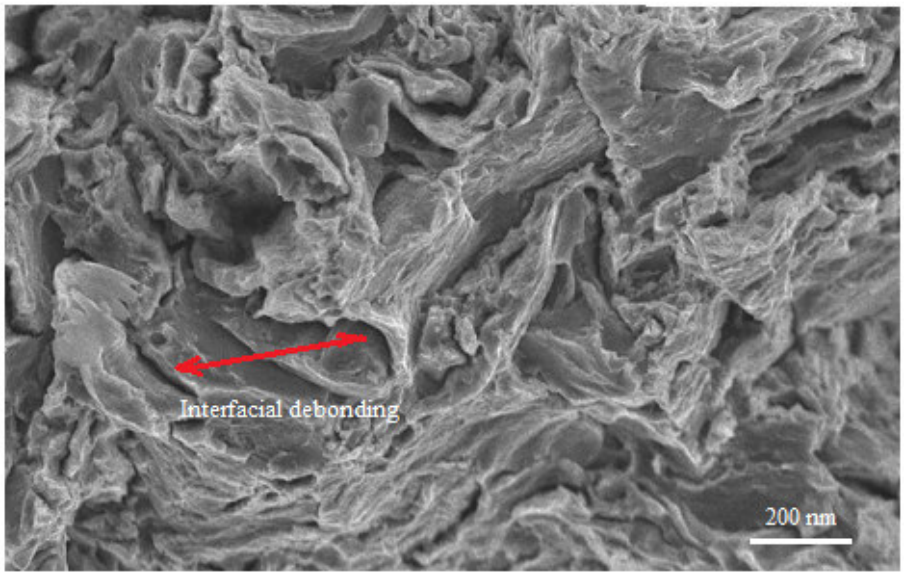

Figure 7: SEM image showing interfacial debonding and cleavage in the matrix.

5. CONCLUSION

The uniform distribution of BN nanoparticles in the AA6061 alloy matrix could be attributed to the closer density values between the AA6061 alloy matrix and BN nanoparticles. The shear stress is high at the interface leading to interfacial debonding in AA6061/BN composites. Due to lack of load transfer from the matrix to the particle, the cleavage in the matrix is also observed.

REFERENCES

1. H. Fujii, H. Nakae, K. Okada, Interfacial reaction wetting in the boron nitride/molten aluminum system, Acta metallurgica and materialia, 41, 1993, pp. 2963-2971.
2. M. Kobashi, T. Choh, Synthesis of boride and nitride ceramics in molten aluminium by reactive infiltration, Journal of Materials Science, 32, 1997, pp. 6283-6289.
3. F.P. Chiaramonte, B.N. Rosenthal, Wettability of pyrolytic boron nitride by aluminum, Journal of the American Ceramic Society, 74, 1991, pp. 658-661.
4. B. Kotiveerachari, A. Chennakesava Reddy, Interfacial effect on the fracture mechanism in GFRP composites, CEMILAC Conference, Ministry of Defence, India, 20-21st August 1999.
5. A. Chennakesava Reddy, Assessment of Debonding and Particulate Fracture Occurrences in Circular Silicon Nitride Particulate/AA5050 Alloy Metal Matrix Composites , National Conference on Materials and Manufacturing Processes, Hyderabad, India, 27-28 February 1998, pp. 104-109.
6. A. Chennakesava Reddy, Evaluation of Debonding and Dislocation Occurrences in Rhombus Silicon Nitride Particulate/AA4015 Alloy Metal Matrix Composites, 1st National Conference on Modern Materials and Manufacturing , Pune, India, 19-20 December 1997, pp. 278-282.
7. S. Sundara Rajan, A. Chennakesava Reddy, Deformation Behavior of AA8090/ TiO_2 Nanoparticulate Reinforced Metal Matrix Composites with Debonding Interfaces, 2nd International Conference on Composite Materials and Characterization, Nagpur, India, 9-10 April 1999, pp. 245-248.
8. A. Chennakesava Reddy, Cohesive Zone Finite Element Analysis to Envisage Interface Debonding in AA7020/Titanium Oxide Nanoparticulate Metal Matrix Composites , 2nd International Conference on Composite Materials and Characterization, Nagpur, India, 9-10 April 1999, pp. 204-209.
9. A. Chennakesava Reddy, Micromechanical Modelling of Interfacial Debonding in AA1100/Graphite Nanoparticulate Reinforced Metal Matrix Composites, 2nd International Conference on Composite Materials and Characterization, Nagpur, India, 9-10 April 1999, pp. 249-253.
10. A. Chennakesava Reddy, Local Stress Differential for Particulate Fracture in AA2024/Titanium Carbide Nanoparticulate Metal Matrix Composites, National Conference on Materials and Manufacturing Processes, Hyderabad, India, 27-28 February 1998, pp. 127-131.
11. B. Kotiveera Chari, A. Chennakesava Reddy, Effect of Debonding on Overall Behavior of AA3003/Titanium Carbide Nanoparticulate Reinforced Metal Matrix Composites, 2nd International Conference on Composite Materials and Characterization, Nagpur, India, 9-10 April 1999, pp. 220-224.
12. H. B. Niranjan, A. Chennakesava Reddy, Effect of Particulate Debonding in AA5050/Boron Nitride Nanoparticulate Reinforced Metal Matrix Composites, 2nd International Conference on Composite Materials and Characterization, Nagpur, India, 9-10 April 1999, pp. 230-234.
13. P. M. Jebaraj, A. Chennakesava Reddy, Interface Debonding Prediction Technique for Tensile Loaded AA6061/Zirconium Oxide Nanoparticulate MMC, 2nd International Conference on Composite Materials and Characterization, Nagpur, India, 9-10 April 1999, pp. 235-239.
14. S. Sundara Rajan, A. Chennakesava Reddy, FEM Model for Volume Fraction Dependent Interface Debonding in TiN Nanoparticle Reinforced AA7020 Metal Matrix Composites, 2nd International Conference on Composite Materials and Characterization, Nagpur, India, 9-10 April 1999, pp. 240-244.
15. A. Chennakesava Reddy, Interfacial Debonding Analysis in Terms of Interfacial Tractions for Titanium Boride/AA3003 Alloy Metal Matrix Composites, 1st National Conference on Modern Materials and Manufacturing , Pune, India, 19-20 December 1997, pp. 124-127.
16. B. Kotiveera Chari, A. Chennakesava Reddy, Interfacial Debonding Analysis in Nanoparticulate Reinforced Metal Matrix Composites of AA8090/Zirconium Carbide, 2nd International Conference on Composite Materials and Characterization, Nagpur, India, 9-10 April 1999, pp. 210-214.
17. H. B. Niranjan, A. Chennakesava Reddy, Debonding Failure and Volume Fraction Effects in Nano-reinforced Composites of AA2024/Silicon Oxide, 2nd International Conference on Composite Materials and Characterization, Nagpur, India, 9-10 April 1999, pp. 215-219.
18. P. M. Jebaraj, A. Chennakesava Reddy, Analysis of Debonding along Interface of AA4015/Magnesium Oxide Nanoparticulate Reinforced Metal Matrix Composites, 2nd International Conference on Composite Materials and Characterization, Nagpur, India, 9-10 April 1999, pp. 225-229.
19. M. Finot, Y. L. Shen, A. Needleman, S. Suresh, Micromechanical modeling of reinforcement fracture in particle-reinforced metal-matrix composites, Metallurgical and Material Transaction, 25A, 1994, pp. 2403-2420.